International Journal of Geo-Information

MDPI

Article

Rapid Evaluation and Validation Method of Above Ground Forest Biomass Estimation Using Optical Remote Sensing in Tundi Reserved Forest Area, India

Praveen Kumar [1], Akhouri P. Krishna [1], Thorkild M. Rasmussen [2] and Mahendra K. Pal [2,*]

[1] Department of Remote Sensing, Birla Institute of Technology, Mesra, Ranchi, Jharkhand 835 215, India; phdrs10054.20@bitmesra.ac.in (P.K.); apkrishna@bitmesra.ac.in (A.P.K.)
[2] Division of Geosciences and Environmental Engineering, Department of Civil, Environmental and Natural Resources Engineering, Luleå University of Technology, Luleå, 971 87 Norrbotten County, Sweden; thorkild.maack.rasmussen@ltu.se
* Correspondence: mahendra.pal@ltu.se; Tel.: +46-(0)920-492434

Abstract: Optical remote sensing data are freely available on a global scale. However, the satellite image processing and analysis for quick, accurate, and precise forest above ground biomass (*AGB*) evaluation are still challenging and difficult. This paper is aimed to develop a novel method for precise, accurate, and quick evaluation of the forest *AGB* from optical remote sensing data. Typically, the ground forest *AGB* was calculated using an empirical model from ground data for biophysical parameters such as tree density, height, and diameter at breast height (*DBH*) collected from the field at different elevation strata. The ground fraction of vegetation cover (*FVC*) in each ground sample location was calculated. Then, the fraction of vegetation cover (*FVC*) from optical remote sensing imagery was calculated. In the first stage of method implementation, the relation model between the ground *FVC* and ground forest *AGB* was developed. In the second stage, the relational model was established between image *FVC* and ground *FVC*. Finally, both models were fused to derive the relational model between image *FVC* and forest *AGB*. The validation of the developed method was demonstrated utilizing Sentinel-2 imagery as test data and the Tundi reserved forest area located in the Dhanbad district of Jharkhand state in eastern India was used as the test site. The result from the developed model was ground validated and also compared with the result from a previously developed crown projected area (*CPA*)-based forest *AGB* estimation approach. The results from the developed approach demonstrated superior capabilities in precision compared to the *CPA*-based method. The average forest *AGB* estimation of the test site obtained by this approach revealed 463 tons per hectare, which matches the previous estimate from this test site.

Keywords: Sentinel-2; regression modeling; fraction of vegetation cover; forest *AGB*

Citation: Kumar, P.; Krishna, A.P.; Rasmussen, T.M.; Pal, M.K. Rapid Evaluation and Validation Method of Above Ground Forest Biomass Estimation Using Optical Remote Sensing in Tundi Reserved Forest Area, India. *ISPRS Int. J. Geo-Inf.* **2021**, *10*, 29. https://doi.org/10.3390/ijgi10010029

Received: 23 November 2020
Accepted: 11 January 2021
Published: 13 January 2021

1. Introduction

Forests are ecosystems maintaining bioresources and providing a range of products and services to meet human needs [1,2]. As reported, 31% of the total Earth's land surface is covered by forests that play a significant role in maintaining ecosystems and providing food, fodder, and shelter. Forests are also instrumental in controlling land degradation by minimizing soil erosion and desertification. Furthermore, even biological diversity in a regional ecosystem is directly affected by surrounding forest cover [3]. Forest biomass is considered reservoirs of carbon. Forests directly have a crucial role in the carbon and water cycle, gross and net primary production (*GPP* and *NPP*), climate changes and global warming, radiation and environment balance, even air quality, and human activities [1,4]. Accurate forest above ground biomass (*AGB*) assessment is crucial for forest resources evaluation, carbon cycle assessment, and sustainable forest management [1–4]. Therefore, forest *AGB* evaluation is essential to recognize possible climate change due to deforestation

and global ecological balance, as well as promoting global biological evolution, community succession, and mitigation processes [1,5,6]. Globally, the rapidly deteriorating forest might be a big threat not only for forest resources but also for future ecological balance [1]. Thus, accurate assessment and monitoring of forest *AGB* for sustainable management and mitigation, and also to recognize climate change scenario due to deforestation are important and crucial [1,5,6]. Forests have great potential to fuel the next generation by harvesting byproducts (e.g., brushwood, lumber, firewood) and supplying a large portion of renewable materials (e.g., edible fruits, nuts, paper, medicinal herbs) that can be converted into renewable energy [1–4,7–9]. The forest biomass evaluation is extremely important to assess renewable energy sources and future planning to keep balance in our environment, economy, and energy security [1–4]. Therefore, forest biomass evaluation and monitoring are crucial to assess the bioresources and terrestrial ecosystem. Forests are considered to be a carbon sink. Forests absorb carbon from the atmosphere through photosynthesis and store it in plant tissue. At a regional as well as global level, estimating the biomass of forest vegetation is an important exercise in determining the storage of carbon in the dominant tree component and computing carbon cycling. It then becomes deposited in forest biomass (that is, trunks, branches, roots, and leaves), in dead organic matter (litter and deadwood), and in soils. This process of carbon absorption and deposition by the forest vegetation is known as carbon sequestration, which can help sustainable management of natural resources. For mitigating CO_2 emissions through carbon sequestration, this driver of climate change has drawn considerable attention to forest ecosystems as a viable option [10].

Globally, the advanced and rapid global observation systems and analyses of geospatial natural resources using remote sensing techniques are being developed. Remote sensing is state-of-the-art, fast, cost-effective, and ecofriendly technique for monitoring and mapping many geospatial natural resources and climate including forest, vegetation water dynamics and change monitoring, and biomass evaluations [1,6,11–14]. Advanced and high-quality data acquisition and distribution facilities are offered by different space organizations, including the National Aeronautics and Space Administration (*NASA*), Canada Centre for Remote Science (*CCRS*) and the European Space Agency (*ESA*) [1,15]. Generally, remote sensing techniques do not derive forest biomass directly but enable acquisition of parameters for forest biomass estimation, such as forest height, leaf area index, the fraction of vegetation cover (*FVC*), or net primary production. Today, due to relatively higher accuracy than conventional systems, fast and cost-effective performance remote sensing systems have gained much attention in the evaluation of the forest biomass and change assessment. Remote sensing technique usually evaluates biomass and change detection/information indirectly rather than directly by retrieving remotely sensed parameters. These extracted parameters help in evaluating *AGB*, forest, and vegetation mapping and monitoring by integration, inversion, and modeling approaches [1,6,13,14]. Further, high-quality data available from the state-of-the-art sensors onboard recently launched satellites by various space agencies are helpful in modeling ecosystems in an innovative manner, as well as to derive new improved land-based inventory systems for estimation of forest canopy height, biomass, carbon stocks, and spatiotemporal changes with relatively high accuracy [6,13,14]. The availability of Sentinel-2 imagery at high spatial resolution (10 to 60 m) from the Copernicus programme offers a new opportunity to study and evaluate forest bioresources and natural carbon stocks. Currently, remotely sensed multiple datasets through passive and active sources are being acquired from different platforms including spaceborne, airborne, and ground data. These data are being used for the noted applications by utilizing innovative processing approaches with advanced statistical, mathematical, and machine learning skills [11,16,17]. Usually, data from active sensors contain a high signal-to-noise ratio (*S:N*) and better penetration compared to passive sensors. Thus, active systems such as synthetic aperture radar (*SAR*), light detection and ranging (*LIDAR*) can penetrate the canopy of the forests, vegetations, and land covers. Consequently, active remote sensing has become a powerful tool for vertical structural and volumetric measurements of the

forests and biomass. Data from passive sensors have great potential for identification, classification, and mapping of forest cover, types, and vegetation classifications [14,18–20].

Since the last decade, forest resource evaluation and atmospheric investigation were remarkably boosted by remote sensing techniques [11]. These techniques are frequently used for forest *AGB* estimation utilizing various datasets. Microwave data such as *SAR* is useful for texture characteristics and backscattered coefficient information extraction, and optical data such as Sentinel-2 are used for vegetation indices and leaf area index (*LAI*) information extraction [1,14,21]. For example, Sentinel-1 as *SAR* data *C*-band and Sentinel-2 optical imagery at high spatial resolution (10 to 60 m) are available freely from the European Copernicus Programme for effective vegetation and forest mapping and monitoring, biomass estimation, and natural resources assessments [1,11]. Similarly, there are plenty of remote sensing datasets freely available from *NASA*, *ESA*, and other space agencies for the above applications. Different modeling and regression approaches between remote sensing microwave data (viz., Sentinel-1—vertical-vertical (*VV*) and vertical-horizontal (*VH*) polarizations) and optical data (viz., Sentinel-2—*LAI* and normalized difference vegetation index (*NDVI*)) and field data are being developed at present for biomass assessments and ground truth validation [22]. For biophysical structure estimation, microwave data of Sentinel-1 were used to derive *InSAR*-based tree height estimation of a hilly forest. This study indicated a reduction in tree height estimation uncertainty even from an undulated terrain [23]. The optical images provide great potential for multitemporal monitoring, improvement in the classification of the forest type with high spatial resolution, and quick revisit time availability [24]. For example, optical remote sensing images viz. Sentinel-2 have been used by various researchers in forest classification, mapping, and monitoring [18–20,25]. Various approaches and experiments are available to extract different parameters in forest *AGB* estimation using optical and microwave remote sensing datasets, including tree height, tree diameter at breast height (*DBH*), and tree volume [25,26]. There are various empirical models and allometric equations developed to estimate forest *AGB* from field data at plot level using hand-measured techniques, viz., tree *DBH*, height, and sometimes wood density to improve accuracy [27]. There are various relational models developed between basal area or tree diameter, weighted height (also known as Lorey′s height) parameters, and *AGB* for more accurate biomass evaluation [28–30], and direct forest *AGB* achieved from *SAR* and *LiDAR* data using the above models from large areas [7,31–33]. Similarly, optical remote sensing studies show that *LAI*, *FVC*, and vegetation indices have significant potential to evaluate forest *AGB* [34]. The *FVC* and *LAI* have proved useful in leaf biomass evaluation through a proportionality function [35]. Usually, *AGB* using field data at the plot level calculates the sum of foliage and wood biomass [36]. To calculate the *LAI* or *FVC*, several vegetation indices have been experimented [37–39], which are still challenging for specific forest types. Furthermore, the accuracy of the *AGB* estimation from both optical and microwave remote sensing data is limited by the accuracy level of data processing and parameter extraction, including ecological, biotic, and topographic factors [6,13,14,22–26,40–42]. In this study, an empirical model based on field *AGB* and *FVC* from optical remote sensing has been worked to simplify and more rapidly evaluate forest *AGB*. The field information (tree height, tree *DBH*, number of trees at plot level (30 by 30 m), tree stem density, and *FVC*) were collected for field *AGB* calculation from a test site within the Tundi reserved forest, Jharkhand state of eastern India.

2. Materials and Methods

For the test site within the Tundi reserved forest, the forest *AGB* was assessed using Sentinel-2 imagery. Brief description of the test site, data details, and the proposed methodology respectively follow.

2.1. Study Area

The study area covers 144 km^2 within Tundi reserved forest in Dhanbad District, Jharkhand state, India. This Indian state is one of the richest in biodiversity due to diverse

climatic and physiographic conditions. It spreads from a northwest to northeast direction with the Domunda hills having two heads (tops) on its eastern fringe.

There are a few isolated hills of varying dimensions scattered in the northern half of this district. The area is a typical deciduous forest that has a total forested area of 23,605 km^2 constituting about 29.61% of the total land area of Jharkhand. In India, reserved and protected forests are declared by the respective state governments. In reserved forests, all activities are prohibited unless permitted; it is vice versa in protected forests, i.e., specific activities such as hunting, grazing, etc., are permitted unless prohibited. Out of the total forest land of Jharkhand, 81.28% is under the protected forest and 18.58% is under the reserved forest category.

Geographically, Jharkhand has two major forest categories, namely tropical zone dry forests and tropical zone wet forests [43]. The test site falls under the tropical zone dry forest category and is covered with *Shorea robusta* (local name Sal) as the most predominant tree species, lies within 23°45′40″ to 24°05′50″ N and 85°57′30″ to 86°35′55″ E (Figure 1a). Tundi reserved forests under Dhanbad Forest Division fall under subgroup 5-B, namely northern tropical dry deciduous forest [8]. The Tundi reserve forest cover contains an almost pure crop of *Shorea robusta* saplings and poles. The test site is dominated by minor hillocks with undulating topography; *Shorea robusta* is dominant and constitutes the top story of the forest, with an average height up to 12 m in the test site. Humus is absent except in remote areas where the forest cover is well protected. The area receives typical monsoon-type climate with three marked seasons: hot, rainy, and winter. Humidity is very high during the rainy season and very low during the hot weather. The maximum temperature rises above 45 °C and a hot wind known as "Loo" blows frequently from April to June, until the onset of monsoon. Thunderstorms usually occur in May, accompanied by a temporary fall of a few degrees. Due to heavy industrialization and mining activities, abundant suspended particles and specks of dust are found in the atmosphere during this season. The monsoon usually breaks in the middle of June and continues until the end of September. The average rainfall is between 1100 to 1200 mm.

Geologically, Tundi comprises Precambrian rock, the country rock being quartz-feldspathic schist intruded rather profusely by some igneous bodies, viz., metadolorites and amphibolites. The prominent hill and hillocks in the area comprise mostly dark color, hard, and compact intrusive rocks (mainly amphibolite and metadolorite). The soil and alluvium are derived largely from gneisses and quartz-feldspathic schist. The soil formation in the forest area is shallow to very shallow, and depth on the plain to undulating land rarely exceeds 60 cm (24 inches). It is generally red loam with pockets of clay. Erosion occurs and varies with slope. The topsoil is hard and compact [44].

2.2. Datasets

Sentinel-2 multispectral image (*MSI*)-level-1C product acquired on 4 December 2019, covering the study area has been chosen as test data of optical remote sensing. Figure 1b shows the false-color composite (*FCC*) image from Sentinel-2 (*L1C*) that encompasses the selected test site within the study area. The spatial resolutions vary between 10 to 60 m and spectral resolutions vary between 15 to 180 nm for different bands of the collected Sentinel-2 image (Table 1).

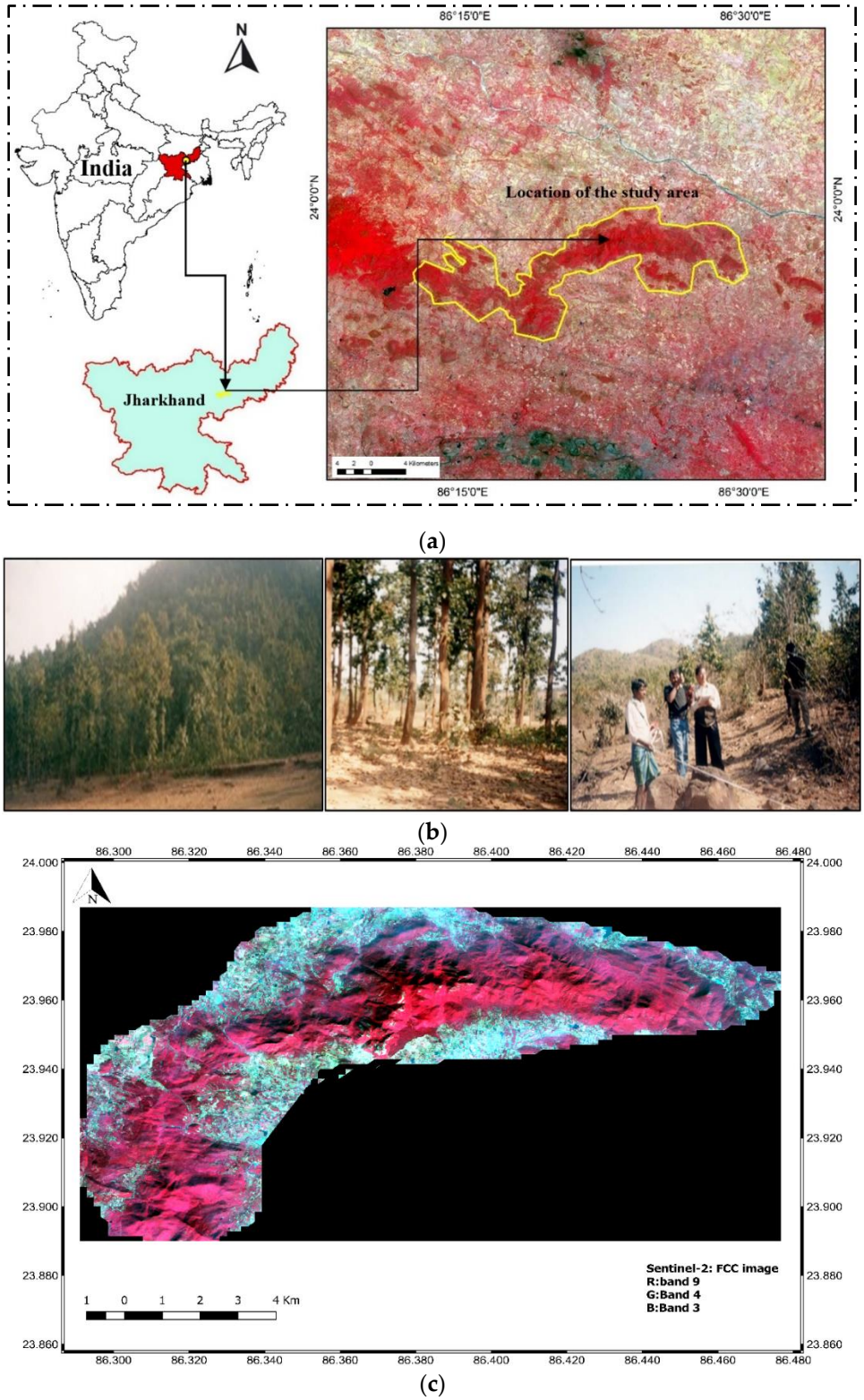

Figure 1. (**a**) Geographic location, (**b**) field photographs, (**c**) false-color composite (*FCC*) image from Sentinel-2 of the study area.

Table 1. Band specification of the Sentinel-2 image.

Subsystem	Band Number	Wavelength Range (μm)	Band Central Wavelength (μm)	Bandwidth (nm)	Spatial Resolution (m)
VNIR	1	0.43–0.45	0.443 (Coastal aerosol)	20	60
	2	0.46–0.52	0.490 (*BLUE*)	65	10
	3	0.54–0.58	0.560 (*GREEN*)	35	
	4	0.65–0.68	0.665 (*RED*)	30	
	5	0.70–0.71	0.705 (Vegetation *RED* edge)	15	20
	6	0.73–0.75	0.749 (Vegetation *RED* edge)	15	
	7	0.77–0.79	0.783 (Vegetation *RED* edge)	20	
	8	0.78–0.90	0.842 (*NIR*)	115	10
	8a	0.86–0.88	0.865 (Vegetation *RED* edge)	20	20
	9	0.93–0.95	0.945 (Water vapor)	20	60
	10	1.37–1.39	1.375 (*SWIR*—Cirrus)	30	
SWIR	11	1.57–1.66	1.610 (*SWIR*)	90	20
	12	2.10–2.28	2.190 (*SWIR*)	180	

Note: *VNIR*, visible and near infrared; *SWIR*, short-wave infrared; *NIR*, near infrared.

Sentinel-2 outperforms other available spaceborne datasets when using near-equivalent image bands when Sentinel-2 data are downsampled to 30 m pixel resolution (for example, Landsat 8). Additionally, Sentinel-2 includes high quality red edge band. Prediction of forest *AGB* using Sentinel-2 confirmed better accuracy compared to Landsat 8 [45]. The field survey was carried out to collect ground forest information for remote sensing-based method development and result validation. In order to cover the complete forest variability of the study area, ground truth locations were chosen randomly based on accessibility in the forest and irrespective to tree height categories. Moreover, ground samples were collected from different locations in such a pattern to cover the entire forest diversity of the study area.

The sample plots selected are a representation of the whole study area. The ground samples were collected from three different profiles separated by nearly 1 km. The distance between samples was also set at approximately 1 km. The ground samples were collected randomly from these profiles based on accessibility into the forest with independent directions. Field data collection was conducted using a global positioning system (*GPS*), altimeter, and ancillary field equipment. The ground samples, including tree height, tree *DBH* and the number of trees per sample plot, tree stem density, and *FVC* from 22 different locations with plot size approximately 30 m × 30 m (approx. 0.09 hectare), were collected from the study site. The field samples from 22 locations comprised approximately 550 individual trees, and an average of 25 trees per plot were measured in different elevation strata. The average measured tree height for each field location was used as tree height of the location for further study. In the ground *FVC* estimation at each sample location, initially, the total number of trees and the radius of each tree cover were calculated. The surface cover of individual trees was assumed circular. Therefore, surface area cover by individual trees was calculated using their covering radius. The total tree cover area at each sample location was estimated by summing individual tree cover area. Lastly, field *FVC* was calculated by taking the ratio of area covered by trees to the total area of the sample

location. Consequently, ground data and *FVC* were utilized for ground *AGB* calculation and validation of the modeled *AGB* from Sentinel-2 data. Further details of the ground data and locations are provided in Table 2. The ground samples sequence provided in Table 2 is the order of data collection regardless of profile composition. Therefore, the sample sequence provided in Table 2 shows random sample location irrespective to spatial pattern of the profile.

Table 2. Details of the ground data from the study area.

Sample Location Number	Easting	Northing	Number of Trees	Average Tree Height (m)	Average *DBH* (cm) (at 4.5 ft Above Ground)
SL1	23°57′53.10″	86°28′23.80″	17	10.9	71.01
SL2	23°58′06.38″	86°23′08.47″	19	23.33	142.49
SL3	23°54′49.91″	86°19′30.53″	24	15.8	80.57
SL4	23°57′58.28″	86°24′18.87″	23	19.7	91.64
SL5	23°57′21.22″	86°22′35.17″	22	17.8	104.33
SL6	23°57′40.13″	86°23′06.37″	20	19.84	95.18
SL7	23°57′05.10″	86°22′26.32″	16	15.55	104.23
SL8	23°53′59.99″	86°18′55.75″	15	17.4	97.02
SL9	23°56′51.50″	86°22′22.10″	16	12.6	92.76
SL10	23°54′53.80″	86°19′35.49″	22	12.86	87.76
SL11	23°58′26.81″	86°25′03.14″	15	9.65	82.56
SL12	23°58′27.79″	86°26′25.76″	17	10.5	77.59
SL13	23°54′51.86″	86°17′49.35″	21	9.8	73.48
SL14	23°58′04.77″	86°27′31.11″	18	13.4	75.88
SL15	23°58′19.68″	86°25′56.25″	19	12.8	75.34
SL16	23°57′39.16″	86°22′51.61″	18	13.6	78.12
SL17	23°57′02.19″	86°19′53.71″	22	14.35	77.62
SL18	23°58′04.77″	86°23′01.88″	27	8.75	67.34
SL19	23°57′37.53″	86°27′11.29″	24	10.8	68.41
SL20	23°56′41.77″	86°20′56.10″	18	13.6	77.78
SL21	23°57′34.62″	86°20′45.56″	16	11.9	71.27
SL22	23°58′18.06″	86°23′36.30″	25	11.85	66.6

2.3. Methodology

The methodology is presented in two phases. In the first phase, a developed general model for forest *AGB* assessment from optical remote sensing imagery is presented, whereas the second phase shows the experimentation of the approach developed specific to the Sentinel-2 image, vegetation indices, and statistical parameters used in this study.

Phase I. Standard procedure for forest *AGB* estimation using optical remote sensing data.

The procedure for estimation of the forest *AGB* was articulated into the following six steps and the flow diagram of the method is shown in Figure 2.

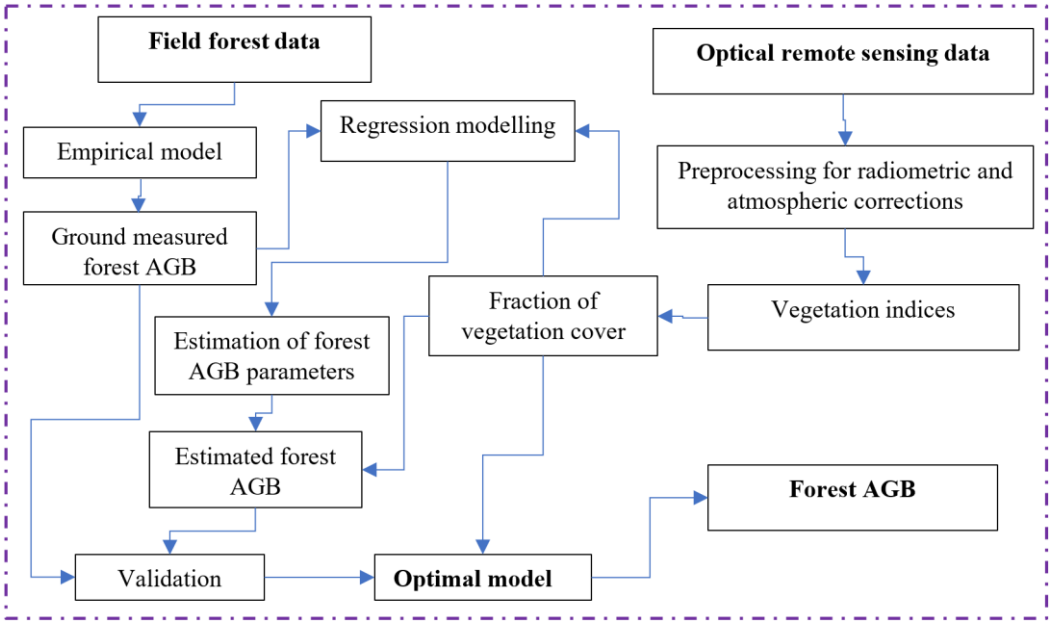

Figure 2. Flow diagram of the proposed methodology.

Step 1: Preprocessing—In this step, the optical remote sensing image was preprocessed for noise reduction, radiometric correction and calibration, atmospheric correction, and spatial resampling. The noise persists in most of the satellite images due to sensor malfunctioning and heating, and environmental influences reduce the quality of the data. Hence, suppression of noise contents in an image is essential to enhance the quality of the data. The distributed remote sensing images usually contain the digital number, which is a calibrated radiance value by sensor-specific gain and offset. Thus, radiometric correction and calibration are required to convert digital numbers to radiance.

Further, atmospheric correction is performed to reduce the effects of atmospheric scattering and absorptions in the radiance data and convert the radiance into reflectance data. The Sentinel-2 image contains different spatial resolution in various spectral bands. Spatial resampling was used to achieve a single spatial resolution from different spatial resolutions in different spectral bands. In preprocessing, noise reduction and radiometric correction were performed using image statistics-based algorithms developed using the gain and offset of the sensor. A combined flat-field and dark object subtraction method was developed for atmospheric correction and conversion of a radiometric image into a reflectance image. The Gram–Schmidt pan sharpening algorithm was used to achieve the entire spectral bands into a single high spatial resolution.

Step 2: Forest *FVC* calculation—In this step, the forest *FVC* at each pixel level was calculated from optical remote sensing imagery using the *FVC* model proposed by Zhang et al. [46] as follows:

Suppose spectral information of pure vegetation pixel and pure soil pixel are represented as S_v and S_s. Then spectral information (S) of an image at each pixel is composed of spectral information of vegetation cover (S_{veg}) and nonvegetation cover (S_o). If forest *FVC* in a pixel is represented as F_c, then a fraction of nonvegetation cover should be $1-F_c$. Thus, mathematically, forest FVC at a pixel level can be calculated as follows:

$$S_{veg} = S_v \times F_c, \tag{1}$$

$$S_o = S_s \times (1 - F_c) \tag{2}$$

$$S = (S_{veg} + S_o) \leftrightarrow \{(S_v \times F_c) + (S_s \times (1 - F_c))\}, \tag{3}$$

$$\text{hence, } F_c = \frac{S - S_s}{S_v - S_s} \tag{4}$$

Using the Equation (4), the *FVC* is calculated from both the optical remote sensing image and field data.

Step 3: Field forest *AGB* estimation—In this step, the field forest *AGB* was calculated from the collected field data. The field forest *AGB* was obtained at individual plot level in kilogram (kg) using the following simplified empirical model proposed by Chave et al. [27] as follows:

$$AGB = \kappa \times \mu D^2 H, \tag{5}$$

where μ is specific gravity (g cm^{-3}) of tree stem, D is the *DBH* (cm), H is the tree height (m), and κ is the constant for forest type.

Step 4: Model development between *FVC* and *AGB*—In this step, linear regression modeling is performed to find the best fit curve between the calculated ground forest *AGB* from field data using Step 3 and the image forest *FVC* obtained using Step 2.

The best fit linear model between the field forest *AGB* and the corresponding image forest *FVC* is represented as follows:

$$AGB = \alpha \times FVC + \beta \tag{6}$$

where α and β are the gain and offset, respectively, for image forest *FVC* used to calculate the forest *AGB*.

Step 5: Forest *AGB* image generation using the forest *FVC* image—Suppose the forest *FVC* image is presented as *FVC*(*i*,*j*) and the image of forest *AGB* is represented as *AGB*(*i*,*j*), where (*i*,*j*) is the pixel location. Then the pixelwise forest *AGB* in kg is calculated as follows:

$$AGB(i,j) = \alpha \times \{FVC(i,j)\} + \beta \tag{7}$$

Step 6: Accuracy assessment—The accuracy of the forest *AGB* calculated from the optical remote sensing image was evaluated by ground validation. The ground validation was performed by comparing the *AGB* value between the field calculated and the image estimate at different ground locations. The accuracy of the result in percentage is represented as:

$$Accuracy\ (\%) = \frac{n}{N} \times 100, \tag{8}$$

where N is the total number of validation points, and n is the number of validation points agreed with when equal or less than one standard deviation between image and field measurements.

Finally, the generalized forest *AGB* obtained by individual plot level in kg are standardized into tons per hectare (t ha^{-1}).

Phase II. Forest *AGB* model evaluation using Sentinel-2 data.

To test and verify the effectiveness of the proposed method, experimentation in sequential procedure was applied on Sentinel-2 as an optical remote sensing image to calculate the forest *AGB* from the Tundi reserved forest test site, Jharkhand, India. The sequential steps in the forest *AGB* calculation are given below.

After preprocessing, the spatial resampling was initially performed to bring all of the spectral bands to 10 m spatial resolution (e.g., bands 2–4 with spatial resolution 10 m and bands 5–7, 8a with spatial resolution 20 m) and then resampled to 30 m spatial resolution, i.e., approximately equal to the field data spatial resolution.

The direct vegetation and nonvegetation (soil) spectral information extraction for the forest *FVC* calculation is tricky. Thus, different vegetation indices were used to quantify the vegetation information within the pixel of an image. In our experiment, for quantifying vegetation amount in a pixel of Sentinel-2, four vegetation indices were assessed: normalized difference vegetation index (*NDVI*), modified vegetation index (*MVI*), soil-adjusted vegetation index (*SAVI*), and modified soil-adjusted vegetation index (*MSAVI*).

The *NDVI*, *MVI*, *SAVI*, and *MSAVI* images were produced from the Sentinel-2 image using the following equations:

$$NDVI = \left(\frac{NIR - RED}{NIR + RED}\right), \tag{9}$$

$$MVI = \sqrt{\frac{(NIR - RED)}{(NIR - RED) + 0.5}} \tag{10}$$

$$SAVI = \frac{(1 + L) \times (NIR - RED)}{(NIR + RED + L)}, \text{ and} \tag{11}$$

$$MSAVI = \frac{\left(2 \times NIR + 1 - \sqrt{(2 \times NIR + 1)^2 - 8 \times (NIR - RED)}\right)}{2} \tag{12}$$

where L is the canopy background adjustment factor (L value as 0.5 in reflectance data) and *NIR* and *RED* are the reflectance values in near infrared and red bands of the multiband remote sensing image.

In our experiment, *NIR* (band 8) and *RED* (band 4) were carefully chosen from the Sentinel-2 reflectance image to calculate these vegetation indices. The highest vegetation index value in an image was considered as a pure vegetation pixel whereas the lowest value was decided as a pure soil pixel. Consequently, pure pixels for vegetation and nonvegetation (soil) information were identified to calculate the forest *FVC* images from the vegetation indices calculated using Equation (4). The best vegetation index among vegetation indices for the forest *AGB* calculation was selected based on the correlation coefficient (R) and mean absolute error (*MAE*) between the ground forest *FVC* and image forest *FVC*. R is the degree of statistical similarity between a pair of variables, whereas *MAE* is a measure of errors between paired observations. R and *MAE* were calculated between the ground *FVC* and the *FVC* from Sentinel-2 by *NDVI*, *MVI*, *SAVI*, and *MSAVI* corresponding to ground sample locations. Based on the highest correlation and lowest *MAE* criteria, the *MSAVI*-based image *FVC* was chosen in *AGB* calculation. Further, the trend line by linear regression between the ground and *MSAVI*-based *FVC* was fitted, which is shown in Equation (13):

$$FVC_{image} = 0.7314 \times FVC_{Ground} + 0.0432 \text{ and } R^2 = 0.9995 \tag{13}$$

In Tundi reserved forest, the predominant tree species is *Shorea robusta* (Sal). Accordingly, based on [27], the ground forest *AGB* was calculated using the following equation from the field data (Table 2):

$$AGB = 0.509 \times \mu D^2 H \tag{14}$$

where *AGB* is the forest above ground biomass (kg), μ (0.667) is specific gravity (tree stem density) (g cm^{-3}), D is the *DBH* (cm), H is the tree height (m), and the constant 0.509 obtained from [27]. The calculated ground forest *AGB* from field data and the selected image forest *FVC* are shown in Table 5.

A trend line is obtained between calculated ground forest *AGB* and image-retrieved forest *FVC* by linear regression. The following model (Equation (15)) was obtained from 15 ground training samples (Table 5) and the remaining 7 ground samples were used for validation of the results obtained from the developed model (Table 6).

$$AGB(i, j) = 92361 \times \{FVC(i, j)\}, \text{ and } R^2 = 0.7494 \tag{15}$$

The accuracy of the forest *AGB* based on Sentinel-2 was assessed by comparing the remaining seven field measurements to the corresponding locations. Kindly note that the samples selected for training were not chosen for the validation to avoid the biasness in the accuracy assessment. Thus, training and validation samples were separated before trend modeling. For data processing and implementation of the proposed procedure and

experimentation in forest *AGB* assessment, mainly the Interactive Data Language (*IDL*) programing and Environment for Visualizing Images (*ENVI*) software were used.

3. Results and Discussion

The forest *AGB* evaluation results from the study area using the methodology and experimental analysis described in Section 2 are produced below.

The estimated forest *FVC* images based on *NDVI*, *MVI*, *SAVI*, and *MSAVI*, respectively, are shown in Figure 3. The ground and image *FVC* calculated from field data and Sentinel-2 respectively, for each vegetation indices extracted from the corresponding locations, are shown in Table 3. The *R* and *MAE* were analyzed between the ground *FVC* and the *FVC* estimated using vegetation indices from Sentinel-2. The estimated *R* and *MAE* values are shown in Table 4. The results show that *MSAVI*-based image *FVC* delivered the highest correlation and lowest *MAE*. Based on the *AGB* empirical model [27], the calculated ground forest *AGB* from field data and the selected image forest *FVC* are shown in Table 5.

Table 3. Ground forest *FVC* and image forest *FVC* calculated from different vegetation indices.

Sample Location Number	*FVC* (*GROUND*)	*FVC* (*NDVI*)	*FVC* (*MVI*)	*FVC* (*SAVI*)	*FVC* (*MSAVI*)
SL1	0.29	0.58	0.56	0.57	0.26
SL2	0.99	0.98	0.97	0.97	0.77
SL3	0.67	0.78	0.77	0.77	0.54
SL4	0.91	0.90	0.90	0.89	0.71
SL5	0.90	0.93	0.92	0.92	0.71
SL6	0.84	0.90	0.90	0.89	0.66
SL7	0.57	0.80	0.80	0.78	0.47
SL8	0.56	0.78	0.77	0.77	0.46
SL9	0.41	0.71	0.70	0.70	0.35
SL10	0.55	0.70	0.68	0.69	0.44
SL11	0.26	0.59	0.56	0.57	0.24
SL12	0.31	0.59	0.57	0.58	0.27
SL13	0.33	0.61	0.57	0.58	0.29
SL14	0.40	0.62	0.60	0.61	0.34
SL15	0.41	0.63	0.60	0.61	0.34
SL16	0.42	0.67	0.64	0.64	0.35
SL17	0.54	0.70	0.67	0.68	0.44
SL18	0.35	0.55	0.50	0.53	0.29
SL19	0.39	0.60	0.56	0.58	0.33
SL20	0.42	0.64	0.62	0.63	0.35
SL21	0.30	0.59	0.56	0.57	0.26
SL22	0.44	0.63	0.59	0.61	0.36

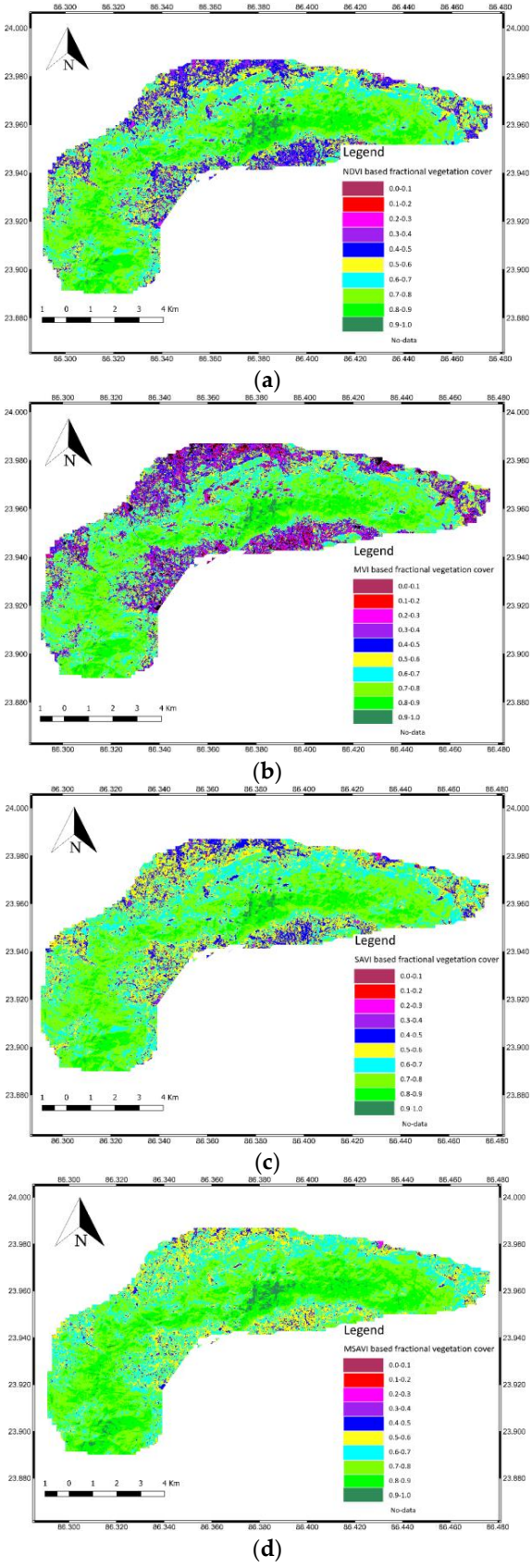

Figure 3. Calculated forest fraction of vegetation cover (*FVC*) images based on (**a**) normalized difference vegetation index (*NDVI*), (**b**) modified vegetation index (*MVI*), (**c**) soil-adjusted vegetation index (*SAVI*), and (**d**) modified soil-adjusted vegetation index (*MSAVI*), from the study area.

Table 4. Correlation coefficient (*R*) and mean absolute error (*MAE*) of image-based forest *FVC* from different vegetation indices with ground forest *FVC*.

Vegetation Indices	*NDVI*	*MVI*	*SAVI*	*MSAVI*
R	0.9696	0.9599	0.9677	0.9981
MAE	0.1941	0.1729	0.1793	0.0947

Table 5. Ground forest *AGB* and selected image forest *FVC*.

Sample Location Number	*AGB* (kg) (Ground)	*FVC* (*MSAVI*)
SL1	18659.89	0.26
SL2	160815.21	0.77
SL3	34821.50	0.54
SL4	56166.84	0.71
SL5	65778.21	0.70
SL6	61020.63	0.66
SL7	57353.44	0.47
SL8	55605.20	0.46
SL9	36807.44	0.35
SL10	33626.20	0.44
SL11	22331.11	0.24
SL12	21460.73	0.27
SL13	17964.20	0.29
SL14	26194.07	0.34
SL15	24666.35	0.34
SL16	28177.79	0.35
SL17	29352.34	0.44
SL18	13470.94	0.29
SL19	17159.58	0.33
SL20	27933.05	0.35
SL21	20521.26	0.26
SL22	17844.75	0.36

As per the derived results from the experimentation using the satellite data together with ground-based primary data, the image-based forest *FVC* was calculated through *MSAVI*. This demonstrated the highest correlation and least mean absolute error with respect to ground *FVC* compared to the other vegetation indices used in this study (Table 4; Figure 3). These comparisons revealed that the *MSAVI* was the best vegetation index for image-based forest *FVC* calculation. Further, image-based forest *FVC* demonstrated a linear relation with a high correlation value of 0.9995 derived using Equation (13).

The empirical model (Equation (14)) was useful in calculating ground forest *AGB*. Further, the linear model between the ground forest *AGB* and selected image-based forest *FVC* showed a good correlation value of 0.75 (Equation (15)). The derived model was applied to the image-based forest *FVC* to calculate image-based *AGB* of the study area (Figure 4). This model was trained using 15 among the 22 samples collected from the field. The accuracy of the Sentinel-2-based forest *AGB* was assessed by comparing the remaining seven field measurements to the corresponding locations. The standard deviation was 3166.50 kg per plot, which was calculated from the forest *AGB* estimate from all 22 locations.

The result shows that all the evaluation between the image-derived and the field calculated forest *AGB* agreed within one standard deviation. The above evaluation was performed based on a single tree species, i.e., *Shorea robusta*. This tree species dominates in the study area by approximately 90%.

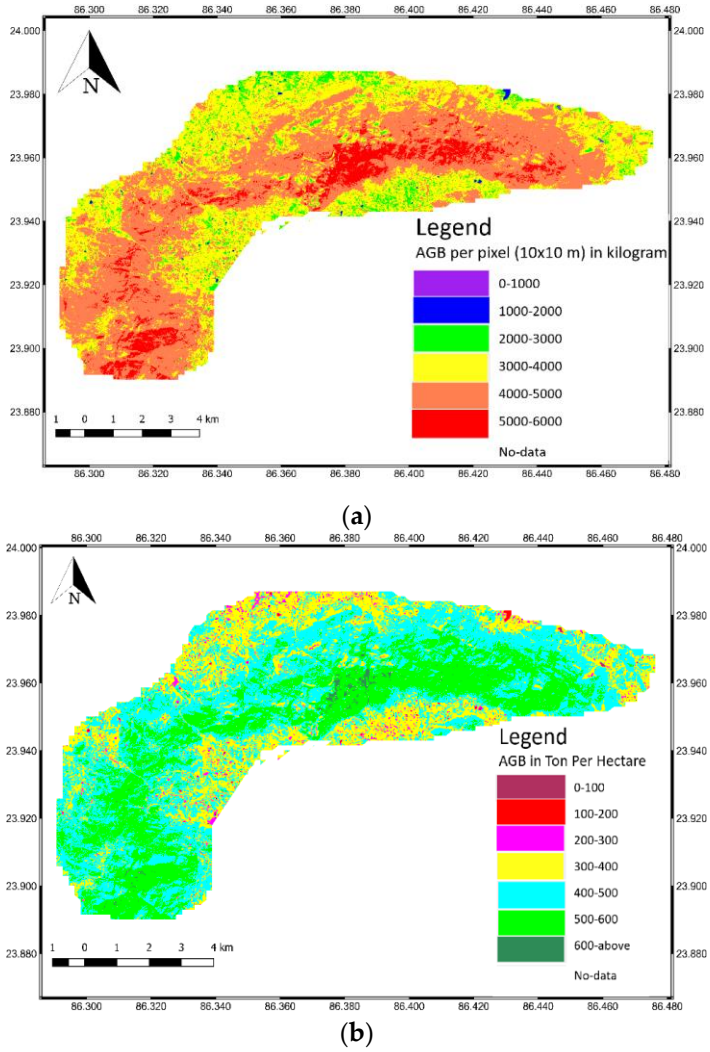

Figure 4. The forest *AGB* calculated from Sentinel-2 imagery in kg per pixel (**a**) and tons per hectare (**b**) for the Tundi reserved forest, Jharkhand, India.

In this study, we have ignored the other tree species to avoid the complexity in the developed method. Thus, we can consider that this study provided approximately more than 90% accuracy. The uncertainty of the final outcome was tested using the chi-squared test. The chi-squared test value was 0.19, i.e., 19% of uncertainty in the estimate.

Finally, the developed model was used to calculate the forest *AGB* of the study area using the Sentinel-2 image (Figure 4). Based on the forest *AGB* map produced, the total calculated forest *AGB* of the study area is estimated at 7,914,875,916.57 kg (7,914,875.92 tons) in 170,704,500 m^2 (17,070.45 hectares). Consequently, the study area contains forest *AGB* on an average of 463.66 tons per hectare.

Further, the efficacy of the method was compared to the Qazi et al. model [47] in forest *AGB* estimates. The Qazi et al. model for forest *AGB* estimate is a linear relationship between crown projected area (*CPA*) achieved from an optical remote sensing image and field based *AGB*.

The model above was derived for Sentinel-2 and ground *AGB* obtained from the study area, which is shown in Equation (16):

$$AGB(i,j) = 17419 \times \{CPA(i,j)\} - 7430.2, \text{ and } R^2 = 0.667 \quad (16)$$

Likewise, the effectiveness of the developed method was compared to the Pandit et al. model [9]. This model was developed based on random forest regression for forest *AGB* estimation. These models were applied to calculated forest *AGB* for the validation, which is shown in Tables 5 and 6.

Table 6. Comparison and validation of the image retrieved forest *AGB* with ground forest *AGB*.

Sample Location Number	Ground *AGB* (in kg)	Image *AGB* (Proposed)	Image *AGB* (Qazi et al. Model)	Image *AGB* (Pandit et al. Model)
SL1	18659.89	18840.10	17989.54	18469.38
SL17	29352.34	30196.83	34432.89	32746.29
SL18	13470.94	14310.09	13934.32	15583.64
SL19	17159.58	17551.79	16930.83	17184.53
SL20	27933.05	28272.18	31030.86	30734.47
SL21	20521.26	19412.03	24418.61	21435.69
SL22	17844.75	18221.16	20692.22	18974.25

The results show that five with Qazi et al. model and six by Pandit et al. model among seven validation points matched within one standard deviation with the ground estimates. Note that the forest *AGB* standard deviation used for comparison was calculated from the total ground data. Further, the potency of the proposed approach was tested using correlation coefficient and mean absolute error.

The results achieved by this approach, the Qazi et al. [47] model, and the Pandit et al. [9] model were evaluated by comparing their outcomes with ground forest *AGB* estimates. The correlation between results from Sentinel-2 image and ground data by the above approach was higher (0.9937) compared to Qazi et al. model (0.9796) and Pandit et al. model (0.9884). Whereas the mean absolute error between outcomes from image and ground data by the proposed approach was lower (582.97) than the Qazi et al. model (18428.41) and the Pandit et al. model (1509.64). The results revealed that the developed approach is superior compared to the Qazi et al. [47] and Pandit et al. [9] models. The forest *AGB* evaluation by the Qazi et al. model was performed by *NDVI*-based *CPA* whereas *AGB* estimation by the proposed approach is achieved by *MSAVI*-based *FVC*. Similarly, a random forest-based regression model was developed for forest *AGB* valuation by Pandit et al. [9]. This model developed a relation between RED-edge-derived vegetation index and ground *AGB* using a random forest algorithm [9].

These results likewise revealed that the selection of the vegetation indices might also be important parameters in forest *AGB* estimation with accuracy. There could be a reason that *MSAVI* is more accurate compared to *NDVI* for vegetation cover recognition in the forest. Moreover, precise *CPA* estimation is difficult compared to *FVC* estimation from optical remote sensing data could be the other reason. Furthermore, the Pandit et al. model revealed that not only robust algorithm selection is valuable, but rather precise vegetation identification and evaluation are also crucial in forest *AGB* model development. However, the developed model considered vegetation index selection for precise forest cover quantification before forest *AGB* model development. The developed approach is straight forward and simple to use for accurate assessment of forest *AGB*. In addition, a generalized forest *AGB* approach is presented so that the developed approach can be applied to other optical remote sensing data for forest *AGB* estimation from different study locations. Overall, these results and analysis from the study area show that Sentinel-2 has

remarkable potential for estimation of the forest *AGB*. Based on the developed approach and the Sentinel-2 image, the average forest *AGB* obtained was 463.66 tons per hectare from the study area, which effectively agreed with the ground observation-based estimates.

One of the key aims of this work was to develop a novel method for precise, accurate, and quick evaluation of the forest above ground biomass from satellite optical remote sensing data. Sentinel-2 satellite data was utilized for this purpose. The ground *FVC* from optical remote sensing imagery at each ground sample location was derived. Apart from various available vegetation indices, a new method has been developed for precise, accurate, and rapid evaluation and validation of above ground forest biomass estimation using optical remote sensing in Tundi reserved forest area, India. This forest area typically represents a subtropical forest type found abundantly in the region for which the study was undertaken. The ground validation and comparisons with the developed *CPA* were validated. This method demonstrated better results than any other known method developed so far. Using this method, *AGB* was derived to be 463 tons per hectare for the study area and further, the satellite-derived data were also compared with the ground estimated data. Finally, the desired level of accuracy was achieved using the model developed. This leads to understanding and appreciating the value of the research outcome from this work.

This study also revealed that the biophysical variables of the vegetation types obtained from Sentinel-2 are useful in the forest *AGB* calculation using local regression. However, this study assumed that the whole study area is composed of a single tree species, whereas in reality forests are composed of multiple tree species with geospatially varying amounts over undulating terrain conditions. In comparison with available datasets and existing techniques, however, the proposed method is highly useful in rapid forest *AGB* assessment. In addition, the availability of high quality optical multispectral remote sensing data on a global scale, free or at low cost from multiple sources, may help global society for forest *AGB* estimation.

Finally, these results lead to conclude that the model obtained quickly produces the forest *AGB* from optical remote sensing images directly with high accuracy. The use of optical remote sensing data is rapid and simple compared to microwave remote sensing data, which need complex data processing for vegetation biophysical parameters extraction in *AGB* estimation. Further, the previous methods [9,47] and microwave data in the forest AGB calculations depend on multiple factors, such as ecological, biotic, and topographic factors, including actual tree height, diameter, stem density, and shape of tree crown information.

4. Conclusions

The goal of this research was to develop a robust and cost-effective method for rapid forest *AGB* evaluation. Initially, ground *FVC* using a fraction of land cover by trees and image *FVC* using vegetation index from the optical remote sensing data were computed. Next, the ground forest *AGB* was derived from the ground data (tree density, tree height, and tree *DBH*) using an empirical model [27]. Subsequently, a relational model was developed between ground forest *AGB* and remote sensing *FVC* by blending this information by using a linear curve fitting approach.

To estimate the forest *AGB*, the devised model was applied to the *FVC* image derived from the optical remote sensing image. The effectiveness of the approach developed was assessed by utilizing Sentinel-2 imagery as test optical remote sensing data. The Tundi reserved forest area, located in Jharkhand state of eastern India, was selected as a test site for this study. The results obtained by the developed approach demonstrated excellent matching with the results achieved by ground-based estimates. The application of the developed method in Tundi reserved forest revealed that the test site contains forest *AGB* on an average of 463 tons per hectare. The result obtained by the proposed approach matches well with the result reported in previous studies from the study area. The result demonstrated more than a 90% match with the ground measurement.

This study still has a future improvement scope, which will employ topographic information in the developed model.

Author Contributions: All authors have made significant contributions to the manuscript. Conceptualization, Praveen Kumar and Mahendra Kumar Pal; methodology, Praveen Kumar and Mahendra Kumar Pal; software, Praveen Kumar, Mahendra Kumar Pal, Thorkild Maak Rasmussen and Akhouri Pramod Krishna; writing—original draft preparation, Praveen Kumar and Mahendra Kumar Pal; writing—review and editing, Praveen Kumar, Mahendra Kumar Pal, Thorkild Maak Rasmussen and Akhouri Pramod Krishna; formal analysis, Praveen Kumar, Mahendra Kumar Pal, Akhouri Pramod Krishna, and Thorkild Maak Rasmussen; validation, Praveen Kumar, Mahendra Kumar Pal, Akhouri Pramod Krishna and Thorkild Maak Rasmussen; data curation, Praveen Kumar, Mahendra Kumar Pal, Thorkild Maak Rasmussen and Akhouri Pramod Krishna; funding acquisition, Praveen Kumar, Mahendra Kumar Pal, Thorkild Maak Rasmussen and Akhouri Pramod Krishna; supervision, Praveen Kumar, Mahendra Kumar Pal, Thorkild Maak Rasmussen and Akhouri Pramod Krishna; project administration, Praveen Kumar, Mahendra Kumar Pal, Thorkild Maak Rasmussen and Akhouri Pramod Krishna. All authors have read and agreed to the published version of the manuscript.

Funding: There is no external funding available for this research work.

Institutional Review Board Statement: Not applicable.

Informed Consent Statement: Not applicable.

Data Availability Statement: Field based primary data have been used. The satellite data used for this study is freely provided by the 'European Space Agency' (ESA), Copernicus Sentinel-2 archived data, which has been duly acknowledged.

Acknowledgments: The authors would like to thank the 'European Space Agency' for providing freely the Copernicus Sentinel-2 data used in this study.

Conflicts of Interest: The authors declare no conflict of interest.

References

1. Norovsuren, B.; Tseveen, B.; Batomunkuev, V.; Renchin, T. Estimation for forest biomass and coverage using Satellite data in small scale area, Mongolia. In *IOP Conference Series: Earth and Environmental Science*; IOP Publishing: Beijing, China, 2019; Volume 320, p. 012019.
2. Kumar, P.; Krishna, A.P.; Nathawat, M.S.; Singh, C.P.; Mohan, S. Tree height estimation in Tundi Reserved Forest using SAR Interferometry. In Proceedings of the Microwave Remote Sensing of the Atmosphere and Environment V, Goa, India, 7 December 2006; Volume 6410, p. 641004-1.
3. Köhl, M.; Lasco, R.D.; Cifuentes, M.; Jonsson, Ö.; Korhonen, K.; Mundhenk, P.; Návar, J.; Stinson, G. Changes in forest production, biomass and carbon: Results from the 2015 UN FAO Global Forest Resource Assessment. *For. Ecol. Manag.* **2015**, *352*, 21–34.
4. Tian, X.; Yan, M.; van der Tol, C.; Li, Z.; Su, Z.; Chen, E.; Li, X.; Li, L.; Wang, X.; Pan, X.; et al. Modeling forest above-ground biomass dynamics using multi-source data and incorporated models: A case study over the qilian mountains. *Agric. For. Meteorol.* **2017**, *246*, 1–14. [CrossRef]
5. Asner, G.P.; Mascaro, J.; Muller-Landau, H.C.; Vieilledent, G.; Vaudry, R.; Rasamoelina, M.; Hall, J.S.; Van Breugel, M. A universal airborne LiDAR approach for tropical forest carbon mapping. *Oecologia* **2011**, *168*, 1147–1160. [CrossRef] [PubMed]
6. Johnson, D.J.; Needham, J.; Xu, C.; Massoud, E.C.; Davies, S.J.; Anderson-Teixeira, K.J.; Bunyavejchewin, S.; Chambers, J.Q.; Chang-Yang, C.; Chiang, J.; et al. Climate sensitive size-dependent survival in tropical trees. *Nat. Ecol. Evolut.* **2018**, *2*, 1436–1442. [CrossRef] [PubMed]
7. Kumar, A.; Saikia, P.; Saikia, P.; Deka, J.; Bharali, S.; Singha, L.; Tripathi, O.; Khan, M.L. Tree diversity assessment and above ground forests biomass estimation using SAR remote sensing: A case study of higher altitude vegetation of North-East Himalayas, India. *Phys. Chem. Earth Parts A/B/C* **2019**, *111*, 53–64. [CrossRef]
8. Champion, S.H.; Seth, S.K. *A Revised Survey of the Forest Types of India*; Amazon.com, Inc.: Delhi, India, 1968.
9. Pandit, S.; Tsuyuki, S.; Dube, T. Estimating Above-Ground Biomass in Sub-Tropical Buffer Zone Community Forests, Nepal, Using Sentinel 2 Data. *Remote. Sens.* **2018**, *10*, 601. [CrossRef]
10. Komolafe, E.T.; Chukwuka, K.S.; Obiakara, M.C.; Osonubi, O. Carbon stock and sequestration potential of Ibodi monkey forest in Atakumosa, Osun state, Nigeria. *Trees For. People* **2020**, *2*, 100031. [CrossRef]
11. Laurin, G.V.; Balling, J.; Corona, P.; Mattioli, W.; Papale, D.; Puletti, N.; Rizzo, M.; Truckenbrodt, J.; Urban, M. Above-ground biomass prediction by Sentinel-1 multitemporal data in central Italy with integration of ALOS2 and Sentinel-2 data. *J. Appl. Remote Sens.* **2018**, *12*, 016008. [CrossRef]

12. Lefsky, M.A. A global forest canopy height map from the Moderate Resolution Imaging Spectroradiometer and the Geoscience Laser Altimeter System. *Geophys. Res. Lett.* **2010**, *37*, L15401. [CrossRef]
13. Liu, Z.; Liu, P.W.; Massoud, E.; Farr, T.G.; Lundgren, P.; Famiglietti, J.S. Monitoring Groundwater Change in California′s Central Valley Using Sentinel-1 and GRACE Observations. *Geosciences* **2019**, *9*, 436. [CrossRef]
14. Massoud, E.C.; Xu, C.; Fisher, R.A.; Knox, R.G.; Walker, A.P.; Serbin, S.P.; Christoffersen, B.O.; Holm, J.A.; Kueppers, L.M.; Ricciuto, D.M.; et al. Identification of key parameters controlling demographically structured vegetation dynamics in a land surface model: CLM4. 5 (FATES). *Geosci. Model Dev.* **2019**, *12*, 4133–4164. [CrossRef]
15. Running, S.W.; Nemani, R.; Heinsch, F.A.; Zhao, M.; Reeves, M.; Hashimoto, H. A Continuous Satellite-Derived Measure of Global Terrestrial Primary Production. *Bioscience* **2004**, *54*, 547–560. [CrossRef]
16. Arun, D.; Kulkarni, B.L. Random Forest Algorithm for Land Cover Classification. *Int. J. Recent Innov. Trends Comput. Commun.* **2016**, *4*, 58–63.
17. Galidaki, G.; Zianis, D.; Gitas, I.; Radoglou, K.; Karathanassi, V.; Tsakiri–Strati, M.; Woodhouse, G.; Mallinis, G. Vegetation biomass estimation with remote sensing: Focus on forest and other wooded land over the Mediterranean ecosystem. *Int. J. Remote Sens.* **2017**, *38*, 1940–1966. [CrossRef]
18. Çolak, E.; Sunar, A.F. Remote sensing & GIS integration for monitoring the areas affected by forest fires: A case study in Izmir, Turkey. *Int. Arch. Photogramm. Remote Sens. Spat. Inf. Sci.* **2018**, *42*, 165–170.
19. Borrás, J.; Delegido, J.; Pezzola, A.; Pereira, M.; Morassi, G.; Camps-Valls, G. Land use classification from Sentinel-2 imagery. *Rev. Teledetección* **2017**, *48*, 55–66.
20. Immitzer, M.; Vuolo, F.; Einzmann, K.; Ng, W.T.; Böck, S.; Atzberger, C. Suitability of Sentinel-2 Data for Tree Species Classification in Central Europe. *WorldView* **2013**, *2*, 16.
21. Tsolmon, R.; Tateishi, R.; Tetuko, J.S.S. A method to estimate forest biomass and its application to monitor Mongolian Taiga using JERS-1 SAR data. *Int. J. Remote Sens.* **2002**, *23*, 4971–4978. [CrossRef]
22. Chen, L.; Ren, C.; Zhang, B.; Wang, Z.; Xi, Y. Estimation of forest above-ground biomass by geographically weighted regression and machine learning with Sentinel imagery. *Forests* **2018**, *9*, 582. [CrossRef]
23. Kumar, P.; Krishna, A.P. InSAR based Tree Height Estimation of Hilly Forest using Multi-Temporal Radarsat-1 and Sentinel-1 SAR data. *IEEE J. Sel. Top. Appl. Earth Obs. Remote Sens.* **2019**, *12*, 5147–5152. [CrossRef]
24. Puletti, N.; Chianucci, F.; Castaldi, C. Use of Sentinel-2 for forest classification in Mediterranean environments. *Ann. Silvic. Res.* **2017**, *42*, 32–38.
25. Zhang, Y.; Liang, S.; Yang, L. A Review of Regional and Global Gridded Forest Biomass Datasets. *Remote Sens.* **2019**, *11*, 2744. [CrossRef]
26. Li, Y.; Wang, H.; Li, X.B. Fractional vegetation cover estimation based on an improved selective endmember spectral mixture model. *PLoS ONE* **2015**, *10*, e0124608. [CrossRef]
27. Chave, J.; Andalo, C.; Brown, S.; Cairns, M.A.; Chambers, J.Q.; Eamus, D.; Lescure, J.P. Tree allometry and improved estimation of carbon stocks and balance in tropical forests. *Oecologia* **2005**, *145*, 87–99. [CrossRef] [PubMed]
28. Lim, K.; Treitz, P.; Wulder, M.; St-Onge, B.; Flood, M. LiDAR remote sensing of forest structure. *Prog. Phys. Geogr. Earth Environ.* **2003**, *27*, 88–106. [CrossRef]
29. Palace, M.W.; Sullivan, F.B.; Ducey, M.J.; Treuhaft, R.N.; Herrick, C.; Shimbo, J.Z.; Mota-E-Silva, J. Estimating forest structure in a tropical forest using field measurements, a synthetic model and discrete return lidar data. *Remote Sens. Environ.* **2015**, *161*, 1–11. [CrossRef]
30. Saatchi, S.; Harris, N.L.; Brown, S.; Lefsky, A.M.; Mitchard, E.T.A.; Salas, W.; Zutta, B.R.; Buermann, W.; Lewis, S.L.; Hagen, S.; et al. Benchmark map of forest carbon stocks in tropical regions across three continents. *Proc. Natl. Acad. Sci. USA* **2011**, *108*, 9899–9904. [CrossRef] [PubMed]
31. Wu, X.; Wang, X.; Wu, Y.; Xia, X.; Fang, J. Forest biomass is strongly shaped by forest height across boreal to tropical forests in China. *J. Plant Ecol.* **2015**, *8*, 559–567. [CrossRef]
32. Solberg, S.; Naesset, E.; Gobakken, T.; Bollandsås, O.M. Forest biomass change estimated from height change in interferometric SAR height models. *Carbon Balance Manag.* **2014**, *9*, 5. [CrossRef]
33. Yu, Y.; Saatchi, S.; Heath, L.S.; LaPoint, E.; Myneni, R.; Knyazikhin, Y. Regional distribution of forest height and biomass from multisensor data fusion. *J. Geophys. Res. Biogeosci.* **2010**, *115*, 16. [CrossRef]
34. Zhang, G.; Ganguly, S.; Nemani, R.R.; White, M.A.; Milesi, C.; Hashimoto, H.; Wang, W.; Saatchi, S.; Yu, Y.; Myneni, R.B. Estimation of forest aboveground biomass in California using canopy height and leaf area index estimated from satellite data. *Remote Sens. Environ.* **2014**, *151*, 44–56. [CrossRef]
35. Zhang, X.; Kondragunta, S. Estimating forest biomass in the USA using generalized allometric models and MODIS land products. *Geophys. Res. Lett.* **2006**, *33*, 09402. [CrossRef]
36. Berner, L.T.; Law, B.E. Plant traits, productivity, biomass, and soil properties from forest sites in the Pacific Northwest, 1999–2014. *Sci. Data* **2016**, *3*, 160002. [CrossRef] [PubMed]
37. Chen, J.M. Evaluation of Vegetation Indices and a Modified Simple Ratio for Boreal Applications. *Can. J. Remote Sens.* **1996**, *22*, 229–242. [CrossRef]
38. Durante, P.; Martín-Alcón, S.; Gil-Tena, A.; Algeet, N.; Tomé, J.L.; Recuero, L.; Palacios-Orueta, A.; Oyonarte, C. Improving Aboveground Forest Biomass Maps: From High-Resolution to National Scale. *Remote Sens.* **2019**, *11*, 795. [CrossRef]

39. Hansen, M.C.; Potapov, P.V.; Moore, R.; Hancher, M.; Turubanova, S.A.; Tyukavina, A.; Thau, D.; Stehman, S.V.; Goetz, S.J.; Loveland, T.R.; et al. High-Resolution Global Maps of 21st-Century Forest Cover Change. *Science* **2013**, *342*, 850–853. [CrossRef] [PubMed]
40. Asner, G.P.; Hughes, R.F.; Varga, T.A.; Knapp, D.E.; Kennedy-Bowdoin, T. Environmental and Biotic Controls over Aboveground Biomass throughout a Tropical Rain Forest. *Ecosystems* **2009**, *12*, 261–278. [CrossRef]
41. Frolking, S.; Palace, M.W.; Clark, D.B.; Chambers, J.Q.; Shugart, H.H.; Hurtt, G.C. Forest disturbance and recovery: A general review in the context of spaceborne remote sensing of impacts on aboveground biomass and canopy structure. *J. Geophys. Res. Biogeosci.* **2009**, *114*, G00E02. [CrossRef]
42. McEwan, R.W.; Lin, Y.-C.; Sun, I.F.; Hsieh, C.-F.; Su, S.-H.; Chang, L.-W.; Song, G.-Z.M.; Wang, H.-H.; Hwong, J.-L.; Lin, K.-C.; et al. Topographic and biotic regulation of aboveground carbon storage in subtropical broad-leaved forests of Taiwan. *For. Ecol. Manag.* **2011**, *262*, 1817–1825. [CrossRef]
43. Ministry of Environment Forest and Climate Change. *State of Forest Report*; Forest Survey of India (Ministry of Environment Forest and Climate Change, GoI): Uttarakhand, India, 2019; Volume 1, pp. 66–85.
44. Rawat, J.K.; Singh, S.; Mishra, R. *Santhal Pargana Forest Report*; Government of Jharkhand: Ranchi, India, 2010; pp. 15–87.
45. Astola, H.; Häme, T.; Sirro, L.; Molinier, M.; Kilpi, J. Comparison of Sentinel-2 and Landsat 8 imagery for forest variable prediction in boreal region. *Remote. Sens. Environ.* **2019**, *223*, 257–273. [CrossRef]
46. Zhang, S.; Chen, H.; Fu, Y.; Niu, H.; Yang, Y.; Zhang, B. Fractional vegetation cover estimation of different vegetation types in the Qaidam Basin. *Sustainability* **2019**, *11*, 864. [CrossRef]
47. Qazi, W.A.; Baig, S.; Gilani, H.; Waqar, M.M.; Dhakal, A.; Ammar, A. Comparison of forest aboveground biomass estimates from passive and active remote sensing sensors over Kayar Khola watershed, Chitwan district, Nepal. *J. Appl. Remote. Sens.* **2017**, *11*, 26038. [CrossRef]